An attempt to determine the cause of the strong tremor responsible for a rockburst in a hard coal mine based on numerical modeling and spectral parameters

Łukasz Wojtecki[1], Krzysztof Krawiec[2], Mateusz Ćwiękała[3], Grażyna Dzik[4]

[1] *Central Mining Institute – National Research Institute, Katowice, Poland,*
e-mail: lwojtecki@gig.eu (corresponding author), ORCID ID: 0000-0002-4791-9909
[2] *Mineral and Energy Economy Research Institute of the Polish Academy of Sciences, Krakow, Poland,*
e-mail: kris@min-pan.krakow.pl, ORCID ID: 0000-0002-5765-1387
[3] *Polish Mining Group, ROW Hard Coal Mine, Rydułtowy, Poland,*
e-mail: m.cwiekala@pgg.pl, ORCID ID: 0000-0002-8084-7521
[4] *State Mining Authority, Katowice, Poland, e-mail: g.dzik@wug.gov.pl, ORCID ID: 0000-0003-4153-6824*

Abstract: Seismic and rockburst hazards represent significant challenges during the longwall mining of coal seams. One analytical approach to assess the potential for rockburst hazards involves reconstructing the stress conditions within the rock mass. This article reports on the findings from three-dimensional (3D) numerical modeling aimed at examining the distribution of maximum shear stress within the rock mass amid the longwall mining operations of the 703/1 coal seam in a mine situated in the Upper Silesian Coal Basin, Poland which was disrupted by a rockburst incident. On the day of the rockburst, substantial concentrations of maximum shear stress were identified in a thick sandstone layer proximate to the boundary of the overlying 624 coal seam located significantly above the 703/1 coal seam. The calculated maximum shear stress demonstrated an increase of approximately 80% over the values observed in the absence of edge effects. Furthermore, also higher concentration of maximum shear stress was identified within the geologically weaker strata adjacent to the 703/1 coal seam. These observations facilitated the classification of the examined rockburst as a stress-stroke phenomenon. Additionally, the study determined the spectral parameters of the tremor, which possessed an energy of 9.8×10^7 J and triggered the analyzed rockburst. The ratio of the seismic energy of S and P-waves confirmed a shear mechanism in the focus. The scope of inelastic deformation within the focal zone was also quantified. Following the event, the rock mass that had been destressed due to the significant tremor and subsequent rockburst exhibited reduced seismic activity upon the resumption of longwall mining of the 703/1 coal seam.

Keywords: hard coal, longwall mining, rockburst hazard, maximum shear stress, numerical modeling, induced seismicity, seismic source parameters

INTRODUCTION

A rockburst represents a catastrophic event characterized by the sudden and violent rupture of rock masses and their dynamic ejection towards excavations. This phenomenon is prevalent in the underground mining of various mineral deposits and during tunnelling activities globally, as evidenced by numerous studies (e.g. Ortlepp & Stacey 1994, Bukowska 2012, Dubiński 2013, Mazaira & Konicek 2015, Cai 2016, Manouchehrian & Cai 2017, Konicek & Schreiber 2018, Li Z. et al. 2018,

Simser 2019, Wang J. et al. 2021, 2022a, 2022b, He et al. 2022). Rockbursts are typically related to the stress levels in rocks near openings, as noted by Ortlepp and Stacey (1994) and Pu et al. (2018).

Stress-induced rockbursts pose a significant hazard in hard coal mining operations, particularly in the Upper Silesian Coal Basin (USCB) in Poland. These events are often caused by high-stress levels within coal seams, resulting from the deposition depth, tectonics, and edges or remnants from previous mining activity. The boundary between a coal seam's mined and unmined parts is critical in providing structural support to the overlying strata. Significant differences in the geomechanical properties of these two parts lead to substantial deformation in the rock mass. As a result, different stress concentration zones appear depending on the type of structural discontinuities. Such stress-induced zones can be identified and monitored by geophysical methods (Dubiński & Dworak 1989, Scott et al. 2004, Szreder et al. 2008, Chen et al. 2015, Pilecki et al. 2023).

The influence of the edges or remnants on the stress distribution within the rock mass diminishes with an increase in both horizontal and vertical distance from the source, as well as over time. Typically, their effect spans several tens of meters horizontally, with the maximum stress concentration observed to be approximately 20 m towards the unexploited side of the coal seam, as detailed by Dubiński and Konopko (2000). Vertically, the stress enhancement attributed to the edge of the coal seam extends from 60 m above to 160 m below, as per the same authors. In practical mining operations, significant consideration is given to edges or remnants due to their potential impact on stress distribution within the seam. However, their influence on the stress levels in adjacent rock strata is generally not regarded as significant if these features are located at substantial distances from the seam being mined. Despite the temporal diminution of this stress influence, its effects can persist and remain detectable for decades after their formation (Dubiński & Konopko 2000).

A stroke rockburst may occur due to the dynamic load impulse correlated with a strong tremor affecting the sidewall part of the coal seam. This type of rockburst does not require a high level of stress in the coal seam. In hard coal mines, strong tremors are mainly associated with the fracturing of thick layers of strong and compact roof rocks, such as sandstones. Shear and slip are the most common mechanisms in the foci of strong tremors induced in this way (e.g. Stec & Błaszczyk 2008, Stec & Wojtecki 2011, Stec 2012, 2017, Pilecka et al. 2021). Sandstone surrounding edges or remnants of previously mined coal seams can experience significant stress changes. If the stress exceeds the rock's strength, it can result in fractures and, consequently, strong tremors.

Mixed rockbursts, also known as stress-stroke rockbursts, are prevalent in hard coal mines and often predominate (Barański et al. 2012). They occur when a dynamic load impulse resulting from a strong tremor loads a partially stressed sidewall part of a coal seam.

Planned longwall mining in hard coal mines in the USCB requires the determination of the two-dimensional distribution of vertical stress in the coal seam within the panel and its vicinity. Identifying areas of stress concentration in the coal seam allows for appropriate preventive measures to be taken, such as blasting, water injection and drilling. Despite the development of numerous monitoring and prevention methods, rockbursts still occur occasionally. In cases where the coal seam is partially or not stressed, but there is a thick layer of sandstone in the roof strata, there is a possibility of a stress-stroke or stroke rockburst, respectively. Determining the stress state even at greater distances from a mined coal seam can help predict potential areas of instability.

There is growing interest in the numerical modeling of the stress state in the rock mass, and not only in the mined coal seam. Various studies have been carried out around the world to numerically model the stress state in coal mining. The modeling results usually demonstrated a high degree of correlation with the results of in situ measurements, thereby confirming their utility in the analysis of stress distribution in the rock mass surrounding mining operations (Yasitli & Unver 2005, Corkum & Board 2016, Krawiec & Czarny 2017, Li M. et al. 2017, Wang P. et al. 2018, Esterhuizen et al. 2019, Chi et al. 2021, Tang et al. 2021).

The relationship between the occurrence of tremors or rockbursts and zones of stress concentration in the rock mass is the basis for using numerical modeling to assess seismic and rockburst hazards (Zhu et al. 2016, Li Z. et al. 2017, Shen et al. 2020, Wang J. et al. 2020, Li Y. & Mitri 2022). In these zones, rocks deform and often accumulate strain energy.

Seismic source parameters are increasingly used in mining seismology and for the assessment of rockburst hazards. These parameters were analyzed for tremors induced in underground mines (e.g. Gibowicz & Kijko 1994, Trifu et al. 1995, Mendecki ed. 1997, Cai et al. 1998, Domański & Gibowicz 2008, Lizurek & Wiejacz 2011, Nordström et al 2017, Caputa & Rudziński 2019), including those induced in underground hard coal mines (e.g. Dubiński et al. 1996, Stec & Błaszczyk 2008, Wojtecki et al. 2016, 2019, Stec 2017). Seismic source parameters are key characteristics that describe the origin and nature of tremors. Spectral parameters can provide information about the focal mechanism of a tremor. This mechanism is influenced by the stress distribution in the rock mass. The shear mechanism of a tremor is related to the shear stress in the rock mass. When shear stress in the rock mass exceeds the strength of the rock, it can cause shear rupture and slip along the fault plane, leading to a tremor. The slip mechanism is often considered a primary mechanism behind induced strong tremors in underground hard coal mines (e.g. Stec & Błaszczyk 2008, Stec & Wojtecki 2011, Stec 2012, 2017, Pilecka et al. 2021).

The article presents the use of 3D modeling to illustrate the distribution of maximum shear stress in rock mass impacted by multi-seam hard coal mining. The numerical model was built by the Fast Lagrangian Analysis of Continua in 3 Dimensions (FLAC3D). Shear stress directly causes shape deformation in rock layers, and its strong concentrations in the rock mass can significantly influence the occurrence of tremor with a shear mechanism. A tremor with an energy of 9.8×10^7 J occurred on 22nd January 2019 at 23:35 CET, and was approximately located in the designated zone of maximum shear stress concentration. The type of focal mechanism, i.e. whether it was shear or non-shear, was determined based on the analysis of spectral parameters.

The presented studies are a combination of two separate methods to determine the causes of a strong tremor responsible for a rockburst in an active hard coal mine. The use of modeling of maximum shear stress distribution for a larger volume of the rock mass may indicate places of the potential occurrence of strong tremors with a shear mechanism, even if they are located far above the coal seam planned for mining. This makes it possible to estimate the risk of rockbursts of the stroke or stress-stroke type.

STUDY AREA

Geological and mining conditions

The Rydułtowy part of the ROW hard coal mine is one of the oldest mines in the USCB and coal has been extracted there for over 200 years. The mine is situated in the western part of the USCB, specifically in the Jejkowice trough (Fig. 1). The coal seams that were mined were deposited during the Carboniferous period, specifically in the Namurian B and C (seam group 500), as well as in the Namurian A (seam groups 600 and 700). The coal seams are interbedded with alternating deposits of shales, mudstones, and fine-grained sandstones. The overburden contains weakly compact fine and medium-grained sandstones and shales from the Triassic period, clays with small interlayers of sandstone and gypsum from the Tertiary period, and clays, sands, and gravels from the Quaternary period. The maximum exploitation depth of the analyzed mine is currently 1,240 m. Coal seams from group 700 have been mined since 1979, and the extraction of coal seams from group 600 was completed in 1993.

Coal seam No. 703/1 was extracted between 2018 and 2020 using a system with the caving of roof rocks and at a depth of approximately 1,150 m. The longwall face extended 200 m in length and advanced from east to west. The overall length of the longwall panel was 1,274 m, with the thickness of the 703/1 coal seam varying between 1.55 m and 2.3 m. The seam was deposited horizontally across the longwall panel, with an inclination ranging from 0° to 5°.
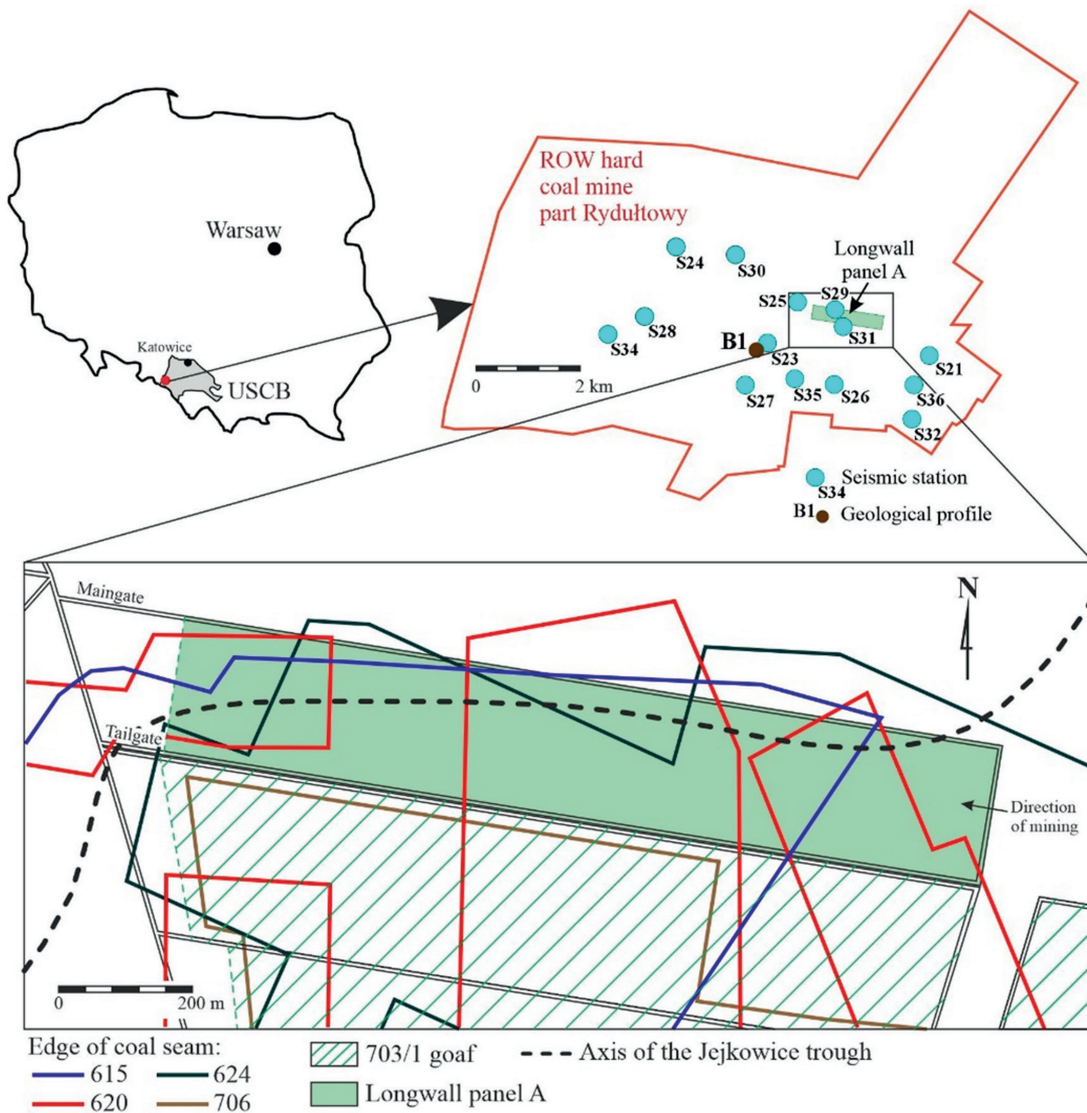
Fig. 1. *Location of the ROW hard coal mine and longwall panel A in the 703/1 coal seam*

The design of the longwall panel predominantly followed the axis of the Jejkowice trough. It is worth noting that the 703/1 coal seam has a uniaxial compressive strength (UCS) of 15 MPa, which is close to the threshold for burst proneness, specifically 16 MPa (Barański et al. 2012). Faults characterized by throws of several to several dozen meters were identified at significant distances from the longwall panel. Additionally, to the south of the tailgate, old goaf resulting from previous exploitation of the 703/1 coal seam were observed. These old goafs were demarcated from longwall panel A by a coal rib up to 5 m in width.

Based on the geological profile (Fig. 2), the thickness of the 703/1 coal seam is 1.6 m. The following rocks are deposited in the direct roof in sequence: shale (0.5 m), hard coal (0.9 m), shale (8 m), sandstone (14 m), sandy shale (2.9 m), hard coal (0.1 m), and sandy shale (10.5 m). The Zamecki sandstone, with a thickness of approximately 60 m, is deposited about 200 m above the 703/1 coal seam. Coal seam No. 624 was deposited about 75 m above the Zamecki sandstone (Fig. 2). The coal seam, which is 1.45 m thick, was partially mined above the longwall panel in the 703/1 coal seam. Similarly, the 620 coal seam, with a thickness of 1.3 m and deposited about 209 m

An attempt to determine the cause of the strong tremor responsible for a rockburst in a hard coal mine...

327

above this thick sandstone layer, was partially extracted above the longwall panel A. At a distance of about 387 m above the Zamecki sandstone, 615 coal seam is deposited. The longwall panel A was mostly under the goaf in 615 coal seam. The vertical distance between coal seams Nos. 624, 620 and 615, and coal seam No. 703/1 is approximately 341 m, 475 m, and 653 m, respectively. It is unlikely that these edges have any influence on the stress level in the 703/1 coal seam. However, the edge of the 624 coal seam may be responsible for the stress increase in the thick layer of Zamecki sandstone.
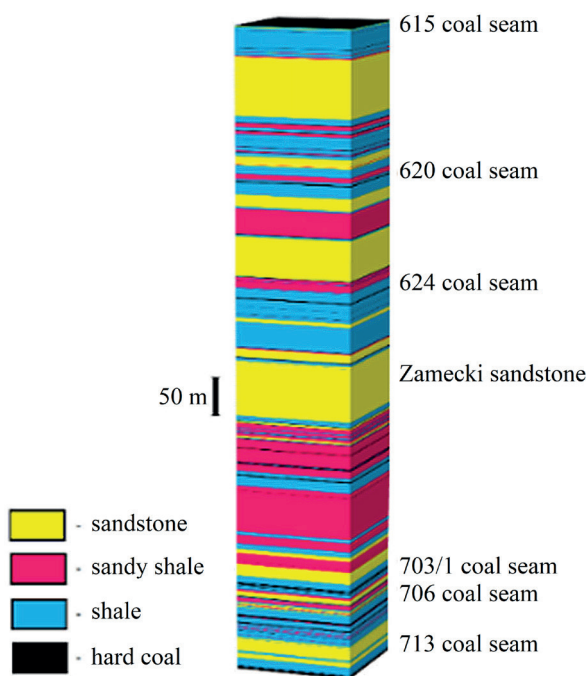

Fig. 2. Geological profile of borehole B1

The direct floor of the 703/1 coal seam contains layers of shale (2.0 m), hard coal (0.6 m), shale (2.9 m), sandy shale (2.5 m), and sandstone (5.65 m). Below it, 705 coal seam (0.95 m thick) is deposited. Deeper layers consist of alternating shale, sandy shale, and sandstone. Coal seam No. 706 (2.15 m thick) is deposited approximately 36 m below the 703/1 coal seam. No coal mining took place below longwall panel A. Coal seam No. 706 was excavated in the southern part of the deposit, at the closest horizontal distance from longwall panel A equals approximately 25 m.

Seismic monitoring and seismic activity

The mining seismology method is one of the techniques used for rockburst hazard assessment in hard coal mines. Seismological observations were conducted during the longwall mining of the 703/1 coal seam using the mine seismological network. The ARAMIS ME system network was used to monitor seismic activity, with a sampling rate of 500 Hz. On the day of the tremor, which had an energy of 9.8×10^7 J and caused the rockburst, the seismic network consisted of low-frequency geophone probes. Apart from one three-component probe, the remaining probes recorded only the vertical component of ground motion. These sensors were located in underground openings at depths ranging from 570 m to 1,205 m below ground level, with a mean depth of −946 m. For the analyzed mine, the ground level is assumed to be approximately 270 m above sea level. The seismic sensors measured the velocity of the vertical component of ground motion. Figure 1 shows the location of the seismic stations in the described seismic network.

The mining tremor coordinates were calculated using the P-wave first arrivals method. The epicenters of tremors that occurred during the mining of the 703/1 coal seam were determined with an error of approximately 11–16 m (mean 13.3 m). The tremor hypocenters were calculated with an error ranging from approximately 30–45 m (mean 37.3 m). The method of the numerical integration of seismograms was used to calculate the energy of tremors. This was based on the seismograms recorded by the seismic sensors described previously. Strong mining-induced tremors can radiate energy across a range of frequencies, including those below 1 Hz. The effectiveness of recording such tremors depends on the capabilities of the sensors in use, including their flat response characteristics. Some sensors may miss very low-frequency components, but overall, strong mining tremors often exhibit a dominant frequency in the range of several hertz. To calculate the energy for each sensor that registered the tremor, we took into account the sum of the squared amplitudes, the density of the rock mass, the attenuation of the rock mass, the calibration factor of the seismic sensor, the hypocenter-sensor distance, and the P-wave

velocity in the rock mass. We then arithmetically averaged these energies, and this average was considered as the final energy.

The local magnitude M_L of tremors was calculated using the formula provided by Dubiński and Wierzchowska (1973):
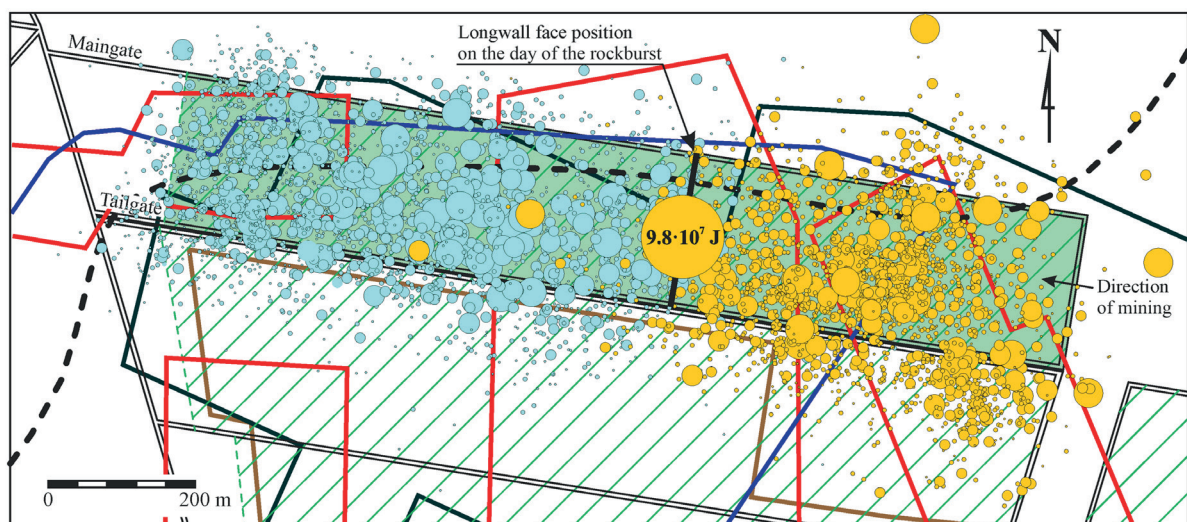
$$\log E = 1.8 + 1.9 M_L \qquad (1)$$

From the beginning of the mining of longwall panel A up to and including the day of the rockburst, the following tremors were recorded (refer to Figure 3): 186 tremors with energy of 10^2 J or less ($M_L < 0.63$), 1,165 tremors with energy of 10^3 J ($0.63 \leq M_L < 1.16$), 413 tremors with energy of 10^4 J ($1.16 \leq M_L < 1.68$), 41 tremors with energy of 10^5 J ($1.68 \leq M_L < 2.21$), 15 tremors with energy of 10^6 J ($2.21 \leq M_L < 2.74$), and one analysed tremor with energy of 9.8×10^7 J ($M_L = 3.26$). A total of 1,821 tremors with a total energy of 2.01×10^8 J were recorded. The rockburst occurred during the longwall face advance of 528 m. The openings were reconstructed over a period of 7 months.

Between the day after the rockburst and the end of longwall mining of the 703/1 coal seam, a total of 1,004 tremors with an energy of 10^2 J or less, 963 tremors with an energy of 10^3 J, 409 tremors with an energy of 10^4 J, 80 tremors with

an energy of 10^5 J, and 32 tremors with an energy of 10^6 J were recorded. A total of 2,488 tremors with a total energy of 1.66×10^8 J were recorded during this period. The seismic activity associated with the mining of longwall panel A is depicted in Figure 3. The tremors in the figure are categorized into two groups: those that occurred before and on the day of the rockburst, and those that occurred after. Additionally, the tremor epicenters are denoted by circles, with the size of each circle reflecting the magnitude of tremor energy. Figure 3 also delineates the edges of distant coal seams Nos. 624, 620, and 615, along with the axis of the Jejkowice trough and the longwall face advance on the day of the rockburst.

The spectral parameters of the tremor, which had an energy of 9.8×10^7 J and caused the rockburst in openings in the 703/1 coal seam, were calculated using seismograms obtained from seismic sensors of the mine seismological network (Fig. 4). The seismological system used has a recording dynamics of 110 dB. The recordings of the three sensors closest to the focus, i.e. at the distances of approximately 190 m, 204 m and 969 m, were clipped (Fig. 4). Seismograms from the remaining sensors located at distances ranging from approximately 1,165 m to 3,567 m were not clipped.

Fig. 3. *Seismic activity during the mining of the longwall panel A in the 703/1 coal seam*
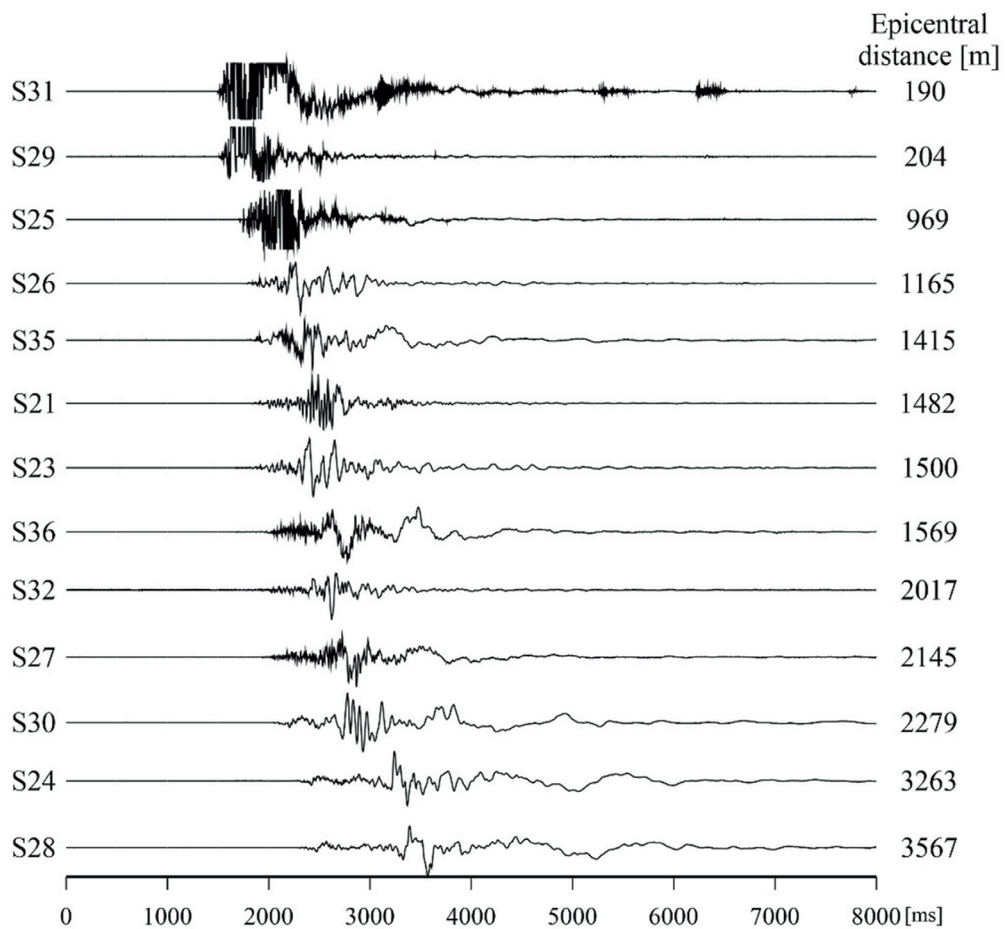
Fig. 4. *Seismograms of the tremor with an energy of 9.8×10^7 J that caused the rockburst*

METHODS

Numerical modeling of shear stress distribution in the rock mass violated by historical exploitation

The use of numerical modeling is becoming increasingly prevalent across a range of disciplines within the geosciences. The modeling methods can be divided into three groups, i.e. continuum, discontinuum and hybrid methods (e.g. Jing 2003). Continuum numerical methods are based on the assumption that the medium is continuous and can be represented by a set of differential equations. The most common continuum numerical methods are the finite element method (FEM), the finite difference method (FDM) and the boundary element method (BEM). Discontinuum numerical methods are used to solve problems involving discontinuous media (e.g. fractured rocks). These methods are based on the assumption that the medium is discontinuous and can be represented by a set of discrete elements. Examples of these methods include the discrete element method (DEM) and discrete fracture network (DFN) method. Hybrid numerical methods assume that the medium is a combination of continuous and discontinuous elements. The main types of hybrid methods are hybrid BEM/FEM, DEM/BEM and DEM/FEM methods.

This article utilizes the finite difference method, a continuum numerical approach, to solve differential equations with given initial and boundary conditions. The rock mass is divided into a finite difference mesh consisting of quadrilateral elements. At discrete points in space, the derivatives in governing equations are directly replaced

by an algebraic expression, such as stresses. The initial boundary problem can be reduced to a system of algebraic equations, where the unknowns are discrete function values.

Numerical modeling of the stress state consists in calculating the stress distribution in a designated part of the mine, e.g. for the selected longwall panel. Current programs make it possible to reconstruct the stress distribution in 3D and for different levels of excavation progress. Therefore, it is possible to estimate the stress state during mining at specific moments. However, it is important to note that numerical modeling is an approximate method. This is because the rock mass is idealized and the locally inhomogeneous and anisotropic properties of the rock mass are often unpredictable and may not be taken into account (Dubiński & Konopko 2000).

The stress distribution in the modelled rock mass can be assessed, for example, on the basis of maximum shear stresses. In general, the maximum shear stress can be determined by using differential stress, expressed as:

$$\tau_{max} = \frac{\sigma_1 - \sigma_3}{2} \tag{2}$$

Shear stress is a critical factor that affects the stability of rock masses. An increase in the maximum shear stress value can lead to a higher risk of violent brittle failure or rockburst in hard rock (Li Y. & Mitri 2022).

Hosseini et al. (2010) and Castro et al. (2012) used numerical modeling to calculate the map of differential stress distribution and identify the rockburst proneness area in the geological and mining conditions of nickel and copper ore mines near Sudbury, Canada. They identified zones with potential for rock mass damage and correlated it with normalized differential stress (NDS):

$$NDS = \frac{\sigma_1 - \sigma_3}{\sigma_c} \tag{3}$$

where: σ_1, σ_3 – the major and minor principal induced stress [MPa], respectively, σ_c – the uniaxial compressive strength of the intact rock [MPa].

Table 1 presents the rock mass damage levels based on the NDS parameter. The stress-based criterion for stress damage and strain-bursting around openings are included, without taking into account loading stiffness (Castro et al. 2012).

Table 1
Rock mass damage levels (Castro et al. 2012)

NDS	Rock mass damage
0.35	no to minor
0.35–0.45	minor (e.g. surface spalling)
0.45–0.6	moderate (e.g. breakout formation)
0.6–0.7	moderate to major
>0.7	major

In order to better understand the distribution of mining-induced stress in the study area, numerical modeling was carried out in the FLAC3D software, which is considered to be the most widely used computer code for stress analysis of rock engineering problems (Müller 1991, Jing 2003, Itasca Consulting Group Inc. 2013, He et al. 2022).

The model geometry was established on the basis of the geological and mining conditions (Fig. 5). The model has dimensions of 1,500 m in length, 1,500 m in width, and 1,100 m in height. A uniform stress of 3.97 MPa was applied to the top of the model, corresponding to 184 m of overburden strata, assuming an overlying unit weight of 2,200 kg/m³. The mesh size is graded depending on the thickness of the strata. The side boundaries were constrained by rollers, and the bottom boundary was fixed both horizontally and vertically. The primary stress was generated by applying gravitational force to all elements. A simple model was used to quantify the stress distribution in the rock mass, so three types of strata were distinguished: sandstone, shale, and coal. The material properties of the rock mass are listed in Table 2, and a Mohr–Coulomb constitutive model was adopted. To simulate bedding separation, particularly near coal seams the interfaces were built into the model using FLAC3D interface logic (Itasca Consulting Group Inc. 2013). The interfaces' mechanical properties, such as shear stiffness k_s and normal stiffness k_n were set to 2×10^{11} Pa and the tensile strength T_i was set to 1×10^{10} Pa (Itasca Consulting Group Inc. 2013).
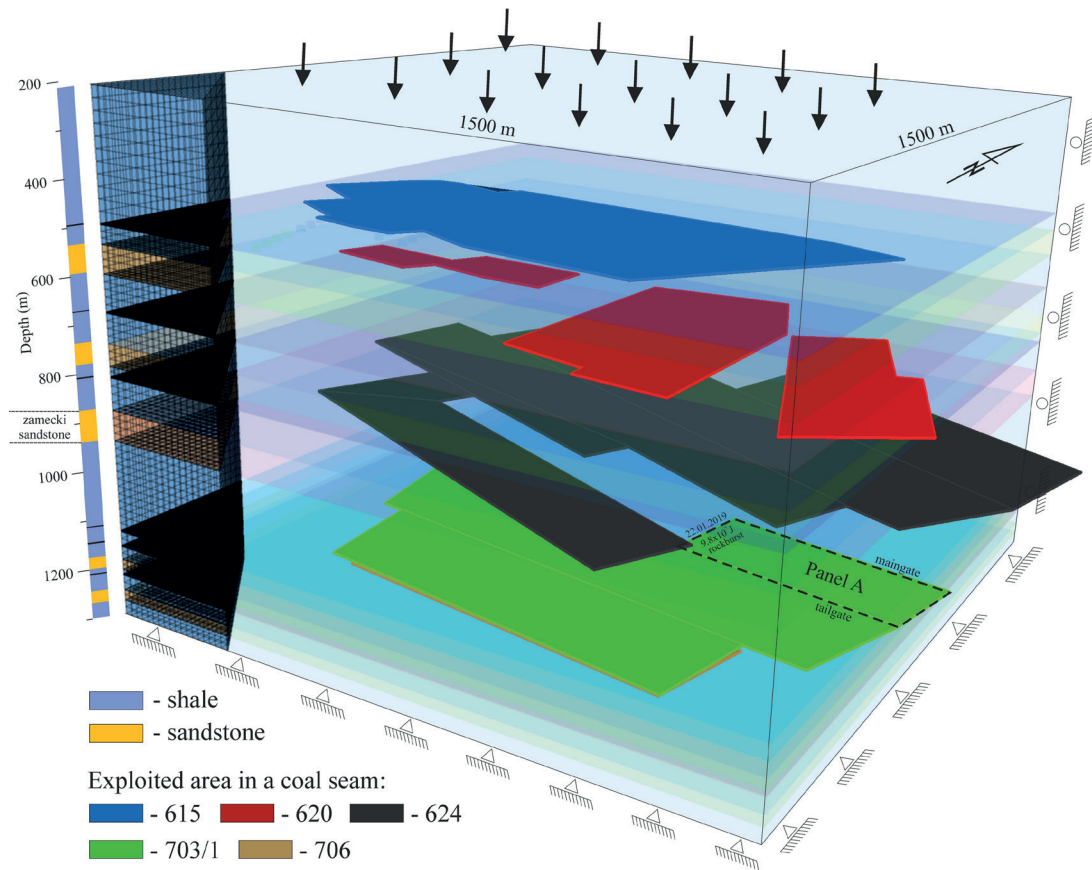
Fig. 5. *Simplified geological profile and numerical model of the studied area*

Table 2
Properties of the rock mass for numerical modeling (Pilecka & Szwarkowski 2018)

Lithology	Volumetric density ρ [kg/m³]	Bulk modulus K [Pa]	Shear modulus G [Pa]	Cohesion c [Pa]	Tension T [Pa]	Friction angle φ [deg]
Sandstone	2,300	1.00E+10	6.68E+9	3.00E+06	2.79E+05	44.05
Zamecki sandstone	2,550	1.78E+10	1.23E+10	3.26E+06	5.51E+05	52.10
Shale	2,400	4.56E+09	2.62E+09	1.60E+06	1.61E+05	26.50
615, 624 coal seams	1,200	5.63E+08	2.30E+08	4.51E+05	2.95E+04	11.85
620 coal seam	1,216	4.45E+08	1.82E+08	1.20E+05	2.95E+04	7.40
703, 706 coal seams	1,250	7.17E+08	2.93E+08	3.82E+05	1.10E+04	14.60
713 coal seam	1,320	7.17E+08	2.93E+08	1.24E+05	4.50E+04	10.50

The excavation process was simulated following the algorithm steps: 1. Calculation of primary stress; 2. Excavation of the longwall panel; 3. Calculation of secondary stress with roof strata subsidence up to a maximum amount equal to the thickness of the seam.

Steps 2 and 3 were repeated for all longwalls from the 615 to 706 coal seams in chronological order according to their mining history. The simulation was interrupted after the longwall panel in the 703/1 coal seam reached the area where a rockburst occurred.

Seismic source parameters

Seismic source parameters are the quantities that describe the focus of the tremor. These parameters can be determined based on the velocity $V(f)$ and displacement $D(f)$ spectra. By integrating the power spectra in the frequency domain, two parameters J and K, are obtained which are the basis for further calculations (Andrews 1986, Snoke 1987, Mendecki ed. 1997, Kwiatek et al. 2016):

$$J = 2\int_0^\infty V^2(f)df \tag{4}$$

$$K = 2\int_0^\infty D^2(f)df \tag{5}$$

In practice, integration takes place in a finite range between frequencies f_1 and f_2. The lower limit is assumed as the reciprocal of the time window, and the upper limit usually corresponds to the Nyquist frequency, defined as a half of the sampling frequency (Gibowicz & Kijko 1994). The spectra of signals from seismic sources show similarity, i.e. the spectrum is practically constant (slightly changing) for low frequencies, and for higher frequencies it decreases proportionally to a certain power. The spectrum can be described by two asymptotes: flat and inclined, i.e. decreasing for high frequencies. The low-frequency level Ω_0 [ms] and the corner frequency f_0 [Hz] are calculated based on the integrals J and K (Andrews 1986, Snoke 1987):

$$\Omega_0 = 2\left(\frac{K^3}{J}\right)^{\frac{1}{4}} \tag{6}$$

$$f_0 = \frac{1}{2\pi}\left(\frac{J}{K}\right)^{\frac{1}{2}} \tag{7}$$

The low-frequency level Ω_0 and the corner frequency f_0 can be determined both for P-wave and S-wave. The low-frequency level Ω_0 corresponds to the flat asymptote, while the corner frequency f_0 corresponds to the intersection of the flat and inclined asymptotes.

The low-frequency level Ω_0 of the tremors causing the rockbursts in the USCB hard coal mines ranged from 1.2×10^{-7} ms to 7.1×10^{-5} ms, while the corner frequency ranged from 2.5 Hz to 6.7 Hz (Dubiński et al. 1996). Other studies of strong tremors in the USCB have found the corner frequency to be between 4.2 Hz and 7.5 Hz (Stec & Błaszczyk 2008).

The low-frequency spectral level Ω_0 is directly related to the seismic moment M_0 [Nm], according to the following formula (Boore & Boatwright 1984, Gibowicz & Kijko 1994):

$$M_0 = \frac{4\pi\rho v_c^3 R\Omega_0}{F_c R_c S_c} \tag{8}$$

where: ρ – rock density in the focus [kg/m³], v_c – P-wave or S-wave velocity [m/s], R – hypocentral distance [m], F_c – radiation pattern coefficient of P-wave or S-wave, R_c – free surface amplification of P-wave or S-wave amplitudes (correction for the radiation), S_c – site correction for P-wave or S-wave.

The seismic moment M_0 calculated for the selected tremors that caused the rockbursts in mines in the USCB achieved for example 8.1×10^{13} Nm (Dubiński et al. 1996). The seismic moment M_0 of strong tremors in one of the coal mines in the USCB was between 4.52×10^{11} Nm and 4.52×10^{13} Nm (Stec & Błaszczyk 2008).

The seismic moment M_0, calculated according to the Formula (8), does not depend on the source model. However, the size of the tremor focus is dependent on the model used. The source radius r_0 [m] is inversely proportional to the corner frequency (Gibowicz & Kijko 1994):

$$r_0 = \frac{kv_c}{2\pi f_0} \tag{9}$$

where k – constant depending on the adopted source model (2.34 for Brune's model, 1.32 for Madariaga's model). Brune's (1970) model assumes a uniform and instantaneous stress drop across the surface of a circular dislocation. Madariaga's (1976) model assumes a plane circular faulting with fixed rupture. The studies of mine tremors conducted by Gibowicz (1984) show that the size of the focus determined on the basis of Madariaga's model correlates with the observations in the mines. The maximum source radius calculated by Dubiński et al. (1996) for the selected tremors that caused rockburst in coal mines in the USCB, and according to Madariaga's model, does not

exceed 200 m. The maximum source radius of strong tremors in one of the hard coal mines in the USCB, calculated by Stec and Błaszczyk (2008) slightly exceeded 100 m.

Based on the seismic moment M_0, the moment magnitude M_w can be calculated according to the following formula (Hanks & Kanamori 1979, Mendecki ed. 1997):

$$M_w = \frac{2}{3} \log\left(M_0\right) - 6.1 \qquad (10)$$

Both M_0 and M_w are equally ranked strength parameters (Gibowicz & Kijko 1994). Based on the seismic moment M_0 and the source radius r_0, the stress drop $\Delta\sigma$ [Pa] can be calculated (Aki & Richards 1980, McGarr et al. 1989, Trifu et al. 1995):

$$\Delta\sigma = \frac{7M_0}{16r_0^3} \qquad (11)$$

The stress drop $\Delta\sigma$ describes the difference between the stress level in the rock mass before and after the tremor. It is determined by the adopted source model, as it depends inversely on the third power of the source radius. This parameter can be used to measure stress release. For selected tremors that caused rockbursts in mines in the USCB, it ranged from one tenth of a megapascal to a maximum of 22 MPa (Dubiński et al. 1996). In the case of other strong tremors in one of the mines in the USCB, the maximum stress drop equaled 17.4 MPa (Stec & Błaszczyk 2008). Seismic events in soft rocks or along existing weak geological features have an average stress drop of approximately 10^4 Pa. For seismic events in hard and highly stressed intact rocks, the stress drop is approximately 10^8 Pa (Mendecki ed. 1997).

One of the seismic source parameters is also seismic energy E_c [J] calculated according to the following formula (Boatwright & Fletcher 1984, Gibowicz & Kijko 1994):

$$E_c = 4\pi\rho v_c \langle R_c \rangle^2 \left(\frac{R}{F_c R_c}\right)^2 \qquad (12)$$

where $\langle R_c \rangle$ is a mean radiation coefficient, and the rest of the markings were described above. The

seismic energy E_c describes the dynamics of the process taking place in the focus. This parameter is calculated differently than the tremor energy described in the previous section. The seismic energy E_c can be calculated on the basis of P- and S-waves independently. These energies are called E_p and E_s, respectively. The ratio of the seismic energies calculated independently for the S- and P-waves, i.e. E_s/E_p, can be an indicator of the type of focal mechanism. For natural earthquakes where the shear process dominates, the ratio is between 10–30 (Boatwright & Fletcher 1984, Boatwright & Quin 1986, Gibowicz & Kijko 1994). It can be assumed that the non-shear mechanism is present in the tremor focus when the E_s/E_p ratio is below 10. In other cases, the shear process should be expected to dominate in the tremor focus. Such a criterion has been applied, for example, for mining tremors in an iron mine (Nordström et al. 2017). Lizurek et al. (2015) obtained an E_s/E_p ratio of 12 for a strong tremor in a copper mine, which may indicate the shear mechanism. Previous studies in copper mines have shown that an E_s/E_p ratio greater than 20 indicates the dominance of the shear, and for lower values, other non-shear processes may be present (Lizurek & Wiejacz 2011). This ratio has also been determined in coal mines for blast induced tremors (Wojtecki et al. 2016, Wojtecki et al. 2019). In this case, the domination or clear participation of shear correlated with a higher value of the E_s/E_p ratio. The highest values of the E_s/E_p ratio were close to 10 (Wojtecki et al. 2019) or slightly above 10 (Wojtecki et al. 2016). The E_s/E_p ratio was also analyzed blast induced tremors in Polish copper mines. The median E_s/E_p ratio for the directly provoked tremors was 0.58, indicating a non-shear mechanism (Caputa & Rudziński 2019). The total radiated seismic energy is a sum of the energy calculated for P-waves and S-waves, however, in the foci of tremors with a shear mechanism, the energy of the S-wave is dominant and is significantly higher than that of the P-wave. In many cases, the P-wave energy is negligible compared to the S-wave energy. In such cases, the total radiated seismic energy is practically equal to the energy of the S-wave.

The radiated energy per unit area per unit slip is another parameter of the seismic source, called

the apparent stress σ_a [J/m³, Pa], and it does not depend on the model used. The formula for calculating σ_a is as follows:

$$\sigma_a = \mu \frac{E_s}{M_0} \qquad (13)$$

where μ is the shear modulus (Wyss & Brune 1968), and assumption that the radiated energy comes from S-wave was made. Based on this parameter, it can be concluded whether the tremor was related to the destruction process in the unfractured or disturbed rock mass. The apparent stress of tremors causing rockbursts in mines in the USCB ranged from 0.015 MPa to 0.17 MPa, and in one individual case it was 1.6 MPa (Dubiński et al. 1996).

Sudden inelastic deformation occurs at the epicenter of the tremor. It can be described by the following parameters: source volume and apparent volume (Mendecki ed. 1997). The source volume V_s [m³] is a volume of coseismic inelastic deformation that radiated the seismic waves (Mendecki ed. 1997). It can be calculated according to the following formula:

$$V_s = \frac{M_0}{\Delta\sigma} \qquad (14)$$

The apparent volume V_a [m³] for a given seismic event measures the volume of rock with coseismic inelastic strain (Mendecki ed. 1997). It is an indicator of the volume of rock affected by inelastic deformation due to the seismic event (Cai et al. 1998), and it is less model dependent than the source volume V_s. Apparent volume V_a can be expressed as follows:

$$V_a = \frac{M_0}{2\sigma_a} \qquad (15)$$

If the apparent volume V_a is assumed to be spherical, then the apparent radius can be determined according to the following formula (Cai et al. 1998):

$$r_a = \sqrt[3]{\frac{3V_a}{4\pi}} \qquad (16)$$

The parameters described above were calculated for the tremor with an energy of 9.8×10^7 J, that caused a rockburst during the mining of the longwall panel A in the 703/1 coal seam in the ROW hard coal mine. The energy ratio E_s/E_p, made it possible to determine the type of mechanism at the focus of the tremor.

RESULTS

Numerical modeling of maximum shear stress distribution

The stress state disturbance caused by the multiseam historical mining of hard coal seams was investigated using a 3D maximum shear stress model. The calculation results are presented on three planes – two vertical planes with an angle between them equal of 100 degrees between them and a horizontal plane located at the level of the longwall panel A. One of the vertical planes passes through the maingate.

The primary and secondary maximum shear stress distributions are shown in Figure 6A and B, respectively. The primary maximum shear stress distribution applies to the case without any mining.

The secondary maximum shear stress distribution describes the situation on the day of the analyzed strong tremor and the resulting rockburst. The longwall face advance of panel A was 528 m. In general, two main anomalies are clearly visible in the 3D model of the secondary stress distribution. Anomaly A is located close to the face of longwall panel A and is directly related to the mining of the 703/1 coal seam. The value of the maximum shear stress in anomaly A reaches a maximum of 13 MPa and is the highest near the old goaf located to the south of longwall panel A. Anomaly B is located about 220 m above the longwall panel A, mainly in the Zamecki sandstone layer. This anomaly clearly correlates with the edge of the 624 coal seam. The increased values of the maximum shear stress extend from the edge of the 624 coal seam to the Zamecki sandstone layer and are V-shaped. The value of the maximum shear stress in anomaly B reaches 11 MPa and is the highest in the Zamecki sandstone layer. This value of maximum shear stress is about 80% higher than the values in Zamecki sandstone in the rest of the area above the longwall panel A.
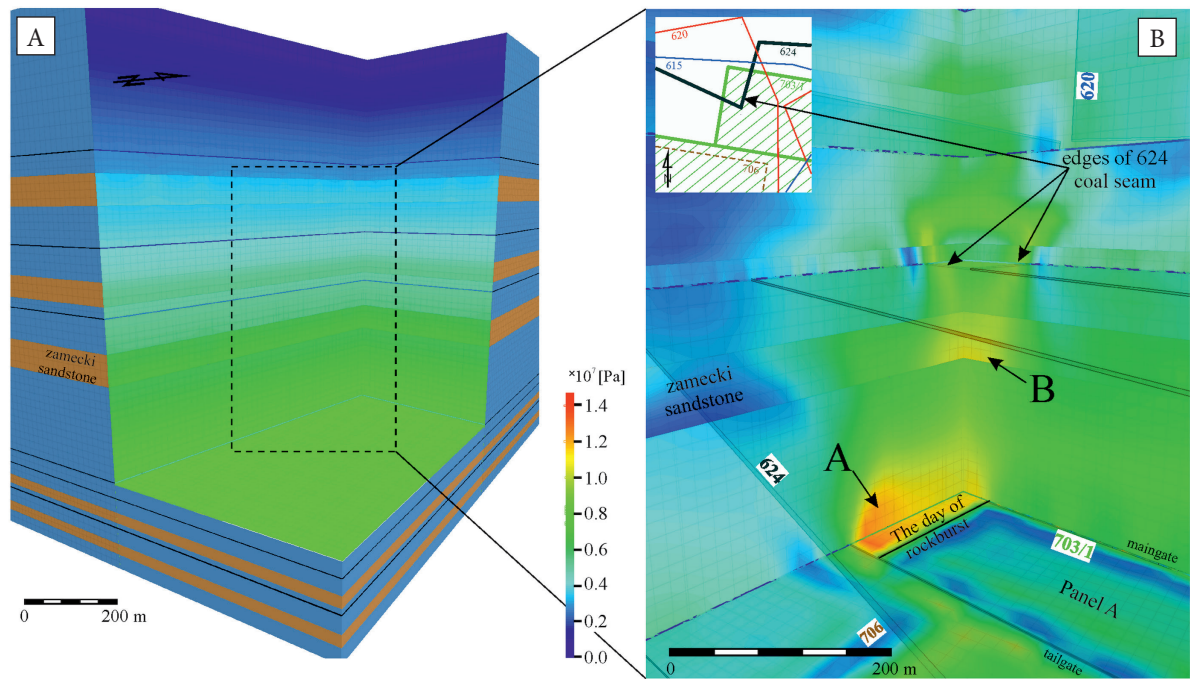
Fig. 6. *Primary maximum shear stress distribution in rock mass without any mining (A) and mining-induced maximum shear stress distribution before the analyzed strong tremor (B)*

Spectral analysis of tremor

Calculations were made individually for each seismic station that recorded a tremor as the cause of a rockburst during longwall mining of the 703/1 coal seam. Basic calculations were performed in the FOCI software (Kwiatek et al. 2016). P- and S-waves were manually marked on the seismograms. Marked parts of the seismograms were then transformed by the Fast Fourier Transformation (FFT). For each P- and S-waves spectrum, the low frequency spectral level Ω_0 and the corner frequency f_0 were determined (Fig. 7). The energy of the P-waves (E_p) and S-waves (E_s) was then calculated and the ratio E_s/E_p was determined. This ratio was 28.1, demonstrating the clear dominance of the shear process in the tremor focus.

The energy of the P-waves was two orders lower than that of the S-waves.

Taking into account the small proportion of P-waves, the remaining spectral parameters were determined on the basis of S-waves only. Table 3 shows the spectral parameters calculated on the basis of S-waves. The parameters from Ω_0 to E_s presented in Table 3 were calculated by averaging the values obtained for each seismogram separately. Applying the formulas from chapter "Seismic source parameters" to the already averaged values, may give different results. The source volume V_s, the apparent volume V_a and the apparent radius r_a have already been calculated on the basis of the averaged parameters given in Table 3 and on the basis of formulas (14), (15) and (16), respectively.

Table 3

Spectral parameters of the tremor that caused the rockburst during mining of longwall panel A in the 703/1 coal seam

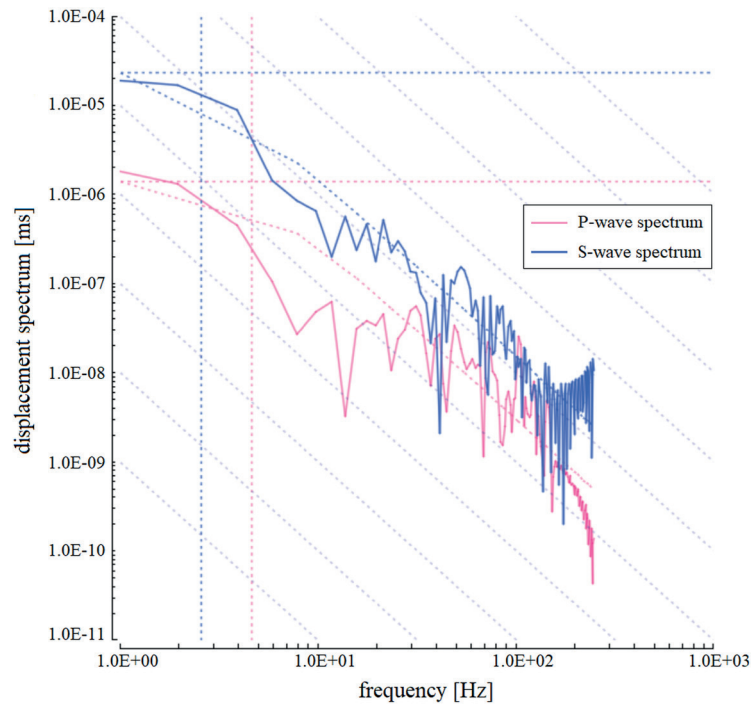| $\Omega_0 \times 10^{-5}$ [ms]	f_0 [Hz]	$M_0 \times 10^{13}$ [Nm]	M_w	r_0 [m]	$\Delta\sigma$ [MPa]	σ_a [MPa]	$E_s \times 10^8$ [J]	E_s/E_p	$V_s \times 10^7$ [m³]	$V_a \times 10^8$ [m³]	r_a [m]
2.06	2.54	3.65	2.95	202.3	1.91	0.0798	1.92	28.1	1.91	2.29	209.5

Fig. 7. *Source displacement spectra of the tremor with energy 9.8×10^7 J*

DISCUSSION

The joint analysis, based on numerical modeling of the maximum shear stress and spectral source parameters, allowed the identification of the most likely causes of the tremor with the energy 9.8×10^7 J, responsible for the rockburst and the destruction in longwall A and its tailgate.

1. The simulation was conducted in a series of phases to systematically reconstruct the chronological sequence of coal seam exploitation near panel A (specifically the 703/1 coal seam) within the Rydułtowy part of the ROW hard coal mine. The final results, accompanied by a graphical depiction of stress distribution, were disclosed at the juncture when the longwall face of panel A attained its position coinciding with the date of the seismic event, which released energy amounting to 9.8×10^7 J, equating to a local magnitude (M_L) of 3.26. As a result of the rockburst, the support for the openings and the nearby infrastructure was destroyed or damaged over a distance of approximately 175 m, i.e. approximately 100 m in the tailgate and 75 m in the longwall face. The results of

numerical calculations of the mining-induced stress state in the rock mass show a large disturbance caused by multi-seam hard coal mining. At the time of the 9.8×10^7 J tremor, excavation of longwall panel A in the 703/1 coal seam was taking place below the edge in the 624 coal seam. It was confirmed that this edge was the cause of increased values of maximum shear stress (up to 11 MPa), particularly in the thick Zamecki sandstone layer. The ongoing mining of the 703/1 coal seam violated the secondary stress equilibrium state established after the exploitation of the 624 coal seam. This led to the release of the energy accumulated in the Zamecki sandstone. The dynamic load correlated with the 9.8×10^7 J tremor that affected the partially stressed 703/1 coal seam and led to a rockburst. The numerical modeling also showed an increased stress level in the area of the longwall face and tailgate (up to 13 MPa). This was most likely caused by the deflection of roof rock over the old goaf left by an excavation of a previous longwall panel in the 703/1 coal seam to the south and by current mining. However, these roof rocks were characterized by lower

values of strength parameters compared to the Zamecki sandstone, and they showed a lower tendency to accumulate strain energy. An analogous state of stress was maintained systematically in the area of the longwall face and tailgate. The rockburst caused by the 9.8×10^7 J tremor was most likely of the stress-strain type.

2. The spectral parameters were used to characterize the focus of the strong tremor with an energy of 9.8×10^7 J. These parameters are increasingly used in mining seismology. Seismic source parameters were calculated and the dominant mechanism in the tremor focus was determined. The shear mechanism in the focus was confirmed. The predominant energy was released from the tremor focus in the form of the transverse seismic waves, as evidenced by the ratio $E_s/E_p = 28.1$. The analyzed tremor was of a regional nature, as evidenced by the value of the seismic moment $M_0 = 3.65 \times 10^{13}$ Nm, the large radius of the focus $r_0 = 202.3$ m, and the high seismic energy $E_s = 1.92 \times 10^8$ J, calculated on the basis of S-waves only. The total energy calculated by adding the energies of P- and S-waves, was about 1.99×10^8 J. The obtained value of the seismic moment M_0 is comparable with the highest values calculated for other strong tremors in the USCB (Stec & Błaszczyk 2008), as well as with other tremors causing rockbursts (Dubiński et al. 1996). However, the source radius is larger than those shown previously, i.e. to the maximum radius of 160 m (Dubiński et al. 1996). The low value of the corner frequency $f_0 = 2.54$ Hz is also noticeable, and it is comparable to the lowest values obtained in previous surveys (Dubiński et al. 1996, Stec & Błaszczyk 2008). For most mining tremors, the stress drop ranges from 0.01 MPa to 10 MPa (Gibowicz & Kijko 1994). In the case of the strong tremor in the ROW hard coal mine, the stress drop was $\Delta\sigma = 1.91$ MPa, indicating that the fracture occurred in hard rather than soft rocks. The apparent stress was $\sigma_a = 0.0798$ MPa. For comparison, the median value of apparent stress of strong tremors at the Rudna copper mine in Poland was 0.052 MPa (Domański & Gibowicz 2008). Several tremors from this copper mine had very similar parameters with the strong tremor in the ROW hard

coal mine, e.g. $f_0 = 2.9$ Hz, $M_0 = 4.48 \times 10^{13}$ Nm, $E_s = 1.08 \times 10^8$ J, $\Delta\sigma = 1.45$ MPa, $\sigma_a = 0.072$ MPa, or $f_0 = 1.9$ Hz, $M_0 = 6.85 \times 10^{13}$ Nm, $E_s = 1.85 \times 10^8$ J, $\Delta\sigma = 0.64$ MPa, $\sigma_a = 0.081$ MPa (Domański & Gibowicz 2008). As mentioned above, the apparent stress is a measure of the seismic energy radiated per unit area per slip. Slip on "smoother" structures is characterized by lower values of apparent stress. Thus, lower values of σ_a may indicate fractures in the existing weak zones, while higher values of apparent stress are correlated with fractures in the undisturbed rock mass. The apparent stress value for the strong tremor in the ROW hard coal mine tends to be higher.

3. An attempt was also made to determine the range of the inelastic deformation in the source of tremor 9.8×10^7 J. For this purpose, the source volume V_s, the apparent volume V_a and the apparent radius r_a were determined. The values of these parameters were 1.91×10^7 m^3, 2.29×10^8 m^3 and 209.5 m, respectively. The source radius, according to Madariaga's model, and the apparent radius, not based on the corner frequency and independent of the model, were almost identical.

4. In the first month after the restart of longwall mining, the total seismic energy released was 1.71×10^6 J, and in the second month it was 6.1×10^6 J. During these two months, the longwall face advance was approximately 111 m. In the following months the longwall face advance was similar, and the mining of the 703/1 coal seam was carried out under analogous geological and mining conditions, but the total monthly seismic energy released was in the order of 10^7 J. The destress effect was no longer present. Lower seismic activity was observed within the designated zones of inelastic deformation and rockburst damages after the reconstruction of the openings and the restart of longwall mining.

CONCLUSIONS

1. Numerical modeling of maximum shear stress can indicate areas in the rock mass where the shear process may occur. Including the numerical modeling of maximum shear stress in the standard assessment of the potential

risk of rockburst hazard could indicate in advance the zones of stress accumulation in the rock mass, and the starting points of the shear process. Stress level can be high in sandstones deformed due to the presence of the edge of previously mined coal seam. These high-stress conditions can contribute to instability and potential failure in these sandstones.

2. Based on the analysis of the spectral parameters, it was found that: shear predominated in the focus of the tremor with the energy of 9.8×10^7 J, and the focus of the tremor responsible for the rockburst in the openings of the 703/1 coal seam was most likely located in the competent rocks with a high value of the shear modulus.

3. The joint application of the numerical modeling of the stress distribution in the rock mass and the spectral source parameters allowed to determine the most likely causes of the tremor that led to the rockburst in the ROW hard coal mine during the longwall mining of the 703/1 coal seam. In particular, the 3D modeling of the distribution of maximum shear stress for different stages of longwall mining seems to be important. Zones of increased maximum shear stress in strong roof rocks may be potential sites for the initiation of strong tremors. Longwall mining in the vicinity of such zones may involve an increased risk of stroke or stress-stroke rockbursts.

4. The calculations presented may prove useful for the planned excavation of coal seams under a thick sandstone layer, even if it is deposited at a much shallower depth.

REFERENCES

Aki K. & Richards P.G., 1980. *Quantitative Seismology: Theory and Methods*. Freeman, San Francisco.

Andrews D.J., 1986. Objective determination of source parameters and similarity of earthquakes of different size. [in:] Das S., Boatwright J. & Scholz C.H. (eds.), *Earthquake Source Mechanics*, Geophysical Monograph Series, 6, American Geophysical Union, Washington, D.C., 259–267. https://doi.org/10.1029/GM037p0259.

Barański A., Drzewiecki J., Dubiński J., Kabiesz J., Konopko W., Kornowski J., Kurzeja J., Lurka A., Makówka J.,

Mutke G. & Stec K., 2012. *Zasady stosowania „Metody kompleksowej i metod szczegółowych oceny stanu zagrożenia tąpaniami w kopalniach węgla kamiennego”*. Instrukcje GIG, 22, Główny Instytut Górnictwa, Katowice.

Boatwright J. & Fletcher J.B., 1984. The partition of radiated energy between P and S waves. *Bulletin of the Seismological Society of America*, 74(2), 361–376. https://doi.org/10.1785/BSSA0740020361.

Boatwright J. & Quin H., 1986. The seismic radiation from a 3-D dynamic model of a complex rupture process. [in:] Das S., Boatwright J. & Scholz C.H. (eds.), *Earthquake Source Mechanics*, Geophysical Monograph Series, 6, American Geophysical Union, Washington, D.C., 97–109.

Boore D.M. & Boatwright J., 1984. Average body-wave radiation coefficients. *Bulletin of the Seismological Society of America*, 74(5), 1615–1621. https://doi.org/10.1785/BSSA0740051615.

Brune J.N., 1970. Tectonic stress and the spectra of seismic shear waves from earthquake. *Journal of Geophysical Research*, 75(26), 4997–5009. https://doi.org/10.1029/JB075i026p04997.

Bukowska M., 2012. The rockbursts in the Upper Silesian Coal Basin in Poland. *Journal of Mining Science*, 48(3), 445–456. https://doi.org/10.1134/S1062739148030070.

Cai M., 2016. Prediction and prevention of rockburst in metal mines – A case study of Sanshandao gold mine. *Journal of Rock Mechanics and Geotechnical Engineering*, 8(2), 204–2011. https://doi.org/10.1016/j.jrmge.2015.11.002.

Cai M., Kaiser P.K. & Martin D., 1998. A tensile model for the interpretation of microseismic events near underground openings. *Pure and Applied Geophysics*, 153(1), 67–92. https://doi.org/10.1007/s000240050185.

Caputa A. & Rudziński Ł., 2019. Source analysis of post-blasting events recorded in deep copper mine, Poland. *Pure and Applied Geophysics*, 176(8), 3451–3466. https://doi.org/10.1007/s00024-019-02171-x.

Castro L.A.M., Bewick R.P. & Carter T.G., 2012. An overview of numerical modeling applied to deep mining. [in:] Ribeiro e Sousa L., Vargas E., Jr., Fernandes M.M. & Azevedo R. (eds.), *Innovative Numerical Modeling in Geomechanics*, CRC Press, London, 393–414. https://doi.org/10.1201/b12130-22.

Chen T., Wang X. & Mukerji T., 2015. In situ identification of high vertical stress areas in an underground coal mine panel using seismic refraction tomography. *International Journal of Coal Geology*, 149, 55–66. https://doi.org/10.1016/j.coal.2015.07.007.

Chi X., Yang K. & Wei Z., 2021. Breaking and mining-induced stress evolution of overlying strata in the working face of a steeply dipping coal seam. *International Journal of Coal Science and Technology*, 8(4), 614–625. https://doi.org/10.1007/s40789-020-00392-3.

Corkum A.G. & Board M.P., 2016. Numerical analysis of longwall mining layout for a Wyoming Trona Mine. *International Journal of Rock Mechanics and Mining Sciences*, 89, 94–108. https://doi.org/10.1016/j.ijrmms.2016.09.001.

Domański B. & Gibowicz S.J., 2008. Comparison of source parameters estimated in the frequency and time domains for seismic events at the Rudna copper mine, Poland. *Acta Geophysica*, 56(2), 324–343. https://doi.org/10.2478/s11600-008-0014-1.

Dubiński J., 2013. The mechanism and consequences of strong mining tremors that occur in Polish hard coal and copper mines. [in:] Kwaśniewski M. & Łydżba D. (eds.), *Rock Mechanics for Resources, Energy and Environment: Proceedings of the ISRM International Symposium (EUROCK 2013)*, Taylor & Francis Group, London, UK, 31–38.

Dubiński J. & Dworak J., 1989. Recognition of the zones of seismic hazard in Polish coal mines by using a seismic method. *Pure and Applied Geophysics*, 129(3–4), 609–617. https://doi.org/10.1007/BF00874528.

Dubiński J. & Konopko W., 2000. *Tąpania: ocena, prognoza, zwalczanie*. Główny Instytut Górnictwa, Katowice.

Dubiński J. & Wierzchowska Z., 1973. *Metody obliczeń energii wstrząsów górotworu na Górnym Śląsku*. Prace Głównego Instytutu Górnictwa. Komunikat, 591, Główny Instytut Górnictwa, Katowice.

Dubiński J., Mutke G. & Stec K., 1996. Focal mechanism and source parameters of the rockbursts in Upper Silesian Coal Basin. *Acta Montana IRSM AS CR*, 9(100), 17–26.

Esterhuizen G.S., Gearhart D.F., Klemetti T., Dougherty H. & van Dyke M., 2019. Analysis of gateroad stability at two longwall mines based on field monitoring results and numerical model analysis. *International Journal of Mining Science and Technology*, 29(1), 35–43. https://doi.org/10.1016/j.ijmst.2018.11.021.

Gibowicz S.J., 1984. The mechanism of large mining tremors in Poland. [in:] Gay N.C. & Wainwright Å.H. (eds.), *Rockbursts and Seismicity in Mines*, South African Institute of Mining and Metallurgy Symposium Series, 6, Southern African Institute of Mining and Metallurgy, Johannesburg, 17–28.

Gibowicz S.J. & Kijko A. 1994. *An Introduction to Mining Seismology*. Academic Press, San Diego.

Hanks T.C. & Kanamori H., 1979. A moment magnitude scale. *Journal of Geophysical Research*, 84(B5), 2348–2350. https://doi.org/10.1029/JB084iB05p02348.

He M., Cheng T., Qiao Y. & Li H., 2022. A review of rockburst: Experiments, theories, and simulations. *Journal of Rock Mechanics and Geotechnical Engineering*, 15(5), 1312–1353. https://doi.org/10.1016/j.jrmge.2022.07.014.

Hosseini Z., Beruar O., Sampson-Forsythe A. & Yao M., 2010. *Mining strategies of multi-sill pillars in burst prone ground conditions at Vale Inco's Coleman Mine* [conference paper]. 44th U.S. Rock Mechanics Symposium and 5th U.S.-Canada Rock Mechanics Symposium, Salt Lake City, Utah, June 2010, ARMA-10-456. https://onepetro.org/ARMAUSRMS/proceedings-abstract/ARMA10/All-ARMA10/ARMA-10-456/118022 [access: 20.03.2024].

Itasca Consulting Group Inc., 2013. *FLAC3D – Fast Lagrangian Analysis of Continua in 3 Dimensions User Manual: Version 5.01*. USA.

Jing L., 2003. A review of techniques, advances and outstanding issues in numerical modeling for rock mechanics and rock engineering. *International Journal of Rock Mechanics and Mining Sciences*, 40(3), 283–353. https://doi.org/10.1016/S1365-1609(03)00013-3.

Konicek P. & Schreiber J., 2018. Heavy rockbursts due to longwall mining near protective pillars: A case study. *International Journal of Mining Science and Technology*, 28(5), 799–805. https://doi.org/10.1016/j.ijmst.2018.08.010.

Krawiec K. & Czarny R., 2017. Comparison of an empirical S-wave velocity model and a calculated stress-strain model for a rock mass disturbed by mining. *E3S Web of Conferences*, 24, 03001. https://doi.org/10.1051/e3sconf/20172403001.

Kwiatek G., Martinez-Garzon P. & Bohnhoff M., 2016. HybridMT: A MATLAB/shell environment package for seismic moment tensor inversion and refinement. *Seismological Research Letters*, 87(4), 964–976. https://doi.org/10.1785/0220150251.

Li M., Zhou N., Zhang J. & Liu Z., 2017. Numerical modeling of mechanical behavior of coal mining hard roofs in different backfill ratios: A case study. *Energies*, 2017(10), 1005. https://doi.org/10.3390/en10071005.

Li Y. & Mitri H.S., 2022. Determination of mining-induced stresses using diametral rock core deformations. *International Journal of Coal Science and Technology*, 9(1), 80. https://doi.org/10.1007/s40789-022-00549-2.

Li Z., He X., Dou L., Song D., 2018. Comparison of rockburst occurrence during extraction of thick coal seams using top-coal caving versus slicing mining methods. *Canadian Geotechnical Journal*, 55(10), 1433–1450. https://doi.org/10.1139/cgj-2016-0631.

Lizurek G. & Wiejacz P., 2011. Moment tensor solution and physical parameters of selected recent seismic events at Rudna copper mine. [in:] Idziak A.F. & Dubiel R. (eds.), *Geophysics in Mining and Environmental Protection*, Geoplanet: Earth and Planetary Sciences, 2, Springer, Berlin, Heidelberg, 11–19. https://doi.org/10.1007/978-3-642-19097-1_2.

Lizurek G., Rudziński Ł. & Plesiewicz B., 2015. Mining induced seismic event on an inactive fault. *Acta Geophysica*, 63(1), 176–200. https://doi.org/10.2478/s11600-014-0249-y.

Madariaga R., 1976. Dynamics of an expanding circular fault. *Bulletin of the Seismological Society of America*, 66(3), 639–666. https://doi.org/10.1785/BSSA0660030639.

Manouchehrian A. & Cai M., 2017. Analysis of rockburst in tunnels subjected to static and dynamic loads. *Journal of Rock Mechanics and Geotechnical Engineering*, 9(6), 1031–1040. https://doi.org/10.1016/j.jrmge.2017.07.001.

Mazaira A. & Konicek P., 2015. Intense rockburst impacts in deep underground construction and their prevention. *Canadian Geotechnical Journal*, 52(10), 1426–1439. https://doi.org/10.1139/cgj-2014-0359.

McGarr A., Bicknell J., Sembera E. & Green R.W.E., 1989. Analysis of exceptionally large tremors in two gold mining districts of South Africa. *Pure and Applied Geophysics*, 129(3–4), 295–307. https://doi.org/10.1007/BF00874511.

Mendecki A.J. (ed.), 1997. *Seismic Monitoring in Mines*. Chapman & Hall, London. https://doi.org/10.1007/978-94-009-1539-8.

Müller W., 1991. Numerical simulation of rockbursts. *Mining Science and Technology*, 12(1), 27, https://doi.org/10.1016/0167-9031(91)91513-h.

Nordström E., Dineva S. & Nordlund E., 2017. Source parameters of seismic events potentially associated with damage in block 33/34 of the Kiirunavaara mine (Sweden). *Acta Geophysica*, 65(6), 1229–1242. https://doi.org/10.1007/s11600-017-0066-1.

Ortlepp W.D. & Stacey T.R., 1994. Rockburst mechanisms in tunnels and shafts. *Tunnelling and Underground Space Technology*, 9(1), 59–65. https://doi.org/10.1016/0886-7798(94)90010-8.

Pilecka E. & Szwarkowski D., 2018. The influence of the fault zone width on land surface vibrations after the high-energy tremor in the "Rydułtowy-Anna" hard coal mine. *E3S Web of Conferences*, 36, 02007. https://doi.org/10.1051/e3sconf/20183602007.

Pilecka E., Stec K., Chodacki J., Pilecki Z., Szermer-Zaucha R. & Krawiec K., 2021. The impact of high-energy mining-induced tremor in a fault zone on damage to buildings. *Energies*, 14(14), 4112. https://doi.org/10.3390/en14144112.

Pilecki Z., Hildebrandt R., Krawiec K., Pilecka E., Lubosik Z. & Łątka T., 2023. Assessment of combustion cavern geometry in underground coal gasification process with the use of borehole ground-penetrating radar. *Energies*, 16(18), 6734. https://doi.org/10.3390/en16186734.

Pu Y., Apel D.B. & Lingga B., 2018. Rockburst prediction in kimberlite using decision tree with incomplete data. *Journal of Sustainable Mining*, 17(3), 158–165. https://doi.org/10.1016/j.jsm.2018.07.004.

Scott D.F., Williams T.J., Tesarik D., Denton I.K., Knoll S.J. & Jordan J., 2004. *Geophysical Methods to Detect Stress in Underground Mines*. Report of Investigations, 9661, U.S. Department of Health and Human Services, Washington.

Shen B., Duan Y., Luo X., van de Werken M., Dlamini B., Chen L., Vardar O. & Canbulat I., 2020. Monitoring and modelling stress state near major geological structures in an underground coal mine for coal burst assessment. *International Journal of Rock Mechanics and Mining Sciences*, 129, 104294. https://doi.org/10.1016/j.ijrmms.2020.104294.

Simser B.P., 2019. Rockburst management in Canadian hard rock mines. *Journal of Rock Mechanics and Geotechnical Engineering*, 11(5), 1036–1043. https://doi.org/10.1016/j.jrmge.2019.07.005.

Snoke J.A., 1987. Stable determination of (Brune) stress drops. *Bulletin of the Seismological Society of America*, 77(2), 530–538.

Stec K., 2012. Focal mechanisms of mine-induced seismic events an explanation of geomechanical processes in the area of Longwall 6, Seam 510 in Hard Coal Mine "Bobrek-Centrum". *Archives of Mining Sciences*, 57(4), 871–886. https://doi.org/10.2478/v10267-012-0057-7.

Stec K., 2017. Określenie przyczyny wysokoenergetycznych wstrząsów górotworu na podstawie parametrów mechanizmu ognisk [Causes of the occurrence of high-energy seismic events based on focal mechanism parameters]. *Zeszyty Naukowe Instytutu Gospodarki Surowcami Mineralnymi i Energią PAN*, 101, 19–32.

Stec K. & Błaszczyk E., 2008. Charakterystyka procesów zachodzących w ogniskach wysokoenergetycznych wstrząsów występujących w czasie eksploatacji ściany 17 w pokładzie 361 w KWK „Knurów" [Characteristics of the processes taking place at the sources of high energy tremors occurring during mining of coalface no. 17 in coal seam no. 361 of the Knurów coal mine]. *Gospodarka Surowcami Mineralnymi*, 24(2/3), 245–259.

Stec K. & Wojtecki Ł., 2011. Charakterystyka mechanizmu ognisk wstrząsów górotworu związanych z eksploatacją pokładu 510 ścianą 502 w kopalni węgla kamiennego Bielszowice [Characteristics of the mine tremor source mechanism associated with the mining in the seam 510, the longwall 502 in the "Bielszowice" coal mine]. *Prace Naukowe GIG. Górnictwo i Środowisko*, 1, 61–77.

Szreder Z., Pilecki Z. & Kłosinski J., 2008. Comparison of Profiling Results of Attenuation and Velocity of Refracted P-wave in Coal-seam. [in:] *Near Surface 2008: 14th European Meeting of Environmental and Engineering Geophysics: 15–17 September 2008 Kraków, Poland: Extended Abstracts & Exhibitors' Catalogue*, European Association of Geoscientists & Engineers, The Netherlands, 1–5. https://doi.org/10.3997/2214-4609.20146265.

Tang Y., Sun W., Zhang X. & Liu P., 2021. Effect of advancing direction of working face on mining stress distribution in deep coal mine. *Advances in Civil Engineering*, 2021(1), 7402164. https://doi.org/10.1155/2021/7402164.

Trifu C.I., Urbancic T.I. & Young R.P., 1995. Source parameters of mining-induced seismic events: An evaluation of homogeneous and inhomogeneous faulting models for assessing damage potential. *Pure and Applied Geophysics*, 145(1), 3–27. https://doi.org/10.1007/BF00879480.

Wang J., Qiu P., Ning J., Zhuang L. & Yang S., 2020. A numerical study of the mining-induced energy redistribution in a coal seam adjacent to an extracted coal panel during longwall face mining: A case study. *Energy Science and Engineering*, 8(3), 817–835. https://doi.org/10.1002/ese3.553.

Wang J., Apel D.B., Pu Y., Hall R., Wei, C. & Sepehri M., 2021. Numerical modeling for rockbursts: A state-of-the-art review. *Journal of Rock Mechanics and Geotechnical Engineering*, 13(2), 457–478. https://doi.org/10.1016/j.jrmge.2020.09.011.

Wang J., Apel D.B., Dyczko A., Walentek A., Prusek S., Xu H. & Wei C., 2022a. Analysis of the damage mechanism of strainbursts by a global-local modeling approach. *Journal of Rock Mechanics and Geotechnical Engineering*, 14(6), 1674–1696. https://doi.org/10.1016/j.jrmge.2022.01.009.

Wang J., Apel D.B., Xu H., Wei C. & Skrzypkowski K., 2022b. Evaluation of the effects of yielding rockbolts on controlling self-initiated strainbursts: A numerical study. *Energies*, 15(7), 2574. https://doi.org/10.3390/en15072574.

Wang P., Zhao J., Feng G. & Wang Z., 2018. Interaction between vertical stress distribution within the goaf and surrounding rock mass in longwall panel systems. *Journal of the Southern African Institute of Mining and Metallurgy*, 118(7), 745. https://doi.org/10.17159/2411-9717/2018/v118n7a8.

Wojtecki Ł., Mendecki M.J. & Zuberek W.M., 2016. The seismic source parameters of tremors provoked by destress blastings in coal seam. *Journal of Mining Science*, 52(2), 258–264. https://doi.org/10.1134/S1062739116020382.

Wojtecki Ł., Konicek P., Mendecki M.J., Gołda I. & Zuberek W.M., 2019. Geophysical evaluation of effectiveness of blasting for roof caving during longwall mining of coal seam. *Pure and Applied Geophysics*, 177(2), 905–917. https://doi.org/10.1007/s00024-019-02321-1.

Wyss M. & Brune J.N., 1968. Seismic moment, stress and source dimensions for earthquakes in the California-Nevada region. *Journal of Geophysical Research*, 73(14), 4681–4694. https://doi.org/10.1029/JB073i014p04681.

Yasitli N.E. & Unver B., 2005. 3-D numerical modeling of stresses around a longwall panel with top coal caving. *Journal of the Southern African Institute of Mining and Metallurgy*, 105(5), 287–300.

Zhu G., Dou L., Li Z., Cai W., Kong Y. & Li J., 2016. Mining-induced stress changes and rockburst control in a variable-thickness coal seam. *Arabian Journal of Geosciences*, 9(5), 365. https://doi.org/10.1007/s12517-016-2356-3.